



# PREPARATION AND CHARACTERIZATION OF GO AND RGO-FILLED LDPE COMPOSITES

Yee Ting Khoo

Faculty of Engineering and Green Technology  
Universiti Tunku Abdul Rahman, Perak, Malaysia

**Abstract** — This study aims to prepare GO and RGO-filled LDPE composites to investigate their barrier properties in hopes to use RGO-filled LDPE as an economical and efficient liner for oil and gas pipelines to prevent corrosion. Graphene oxide (GO) was synthesized from natural graphite flakes by using an improved Hummers method and reduced into reduced graphene oxide (RGO) by chemical reduction using ascorbic acid. FTIR analysis revealed the presence of oxygenated functional groups in the GO and the removal of oxygenated functional groups in the RGO. RGO showed a reduction in hydroxyl groups. LDPE composites containing 0.5 wt% and 1 wt% of GO and RGO were developed through melt mixing. TGA results showed that there was an increase in thermal stability with the addition of filler and that the 1 wt% RGO/LDPE composite had the greatest thermal stability. The mechanical strengths of the composites improved with GO and RGO filler addition. The RGO/LDPE composites exhibited increased tensile strength and Young modulus as well as comparable elongation at break as compared to 100 wt% LDPE and GO/LDPE composites. Morphological analysis through SEM confirmed the presence of agglomeration for both 0.5 wt% and 1 wt% GO/LDPE composites, while both 0.5 wt% and 1 wt% RGO/LDPE composites showed smoother structural morphology with no agglomeration. The RGO/LDPE composites had the best moisture and solvent resistance as compared to the 100 wt% LDPE and GO/LDPE composites. A corrosion test conducted proved that metal plates coated with the 1 wt% RGO/LDPE composite exhibited the best corrosion resistance ability with a corrosion rate of 0%. Thus, the RGO/LDPE composites at 1 wt% RGO loading is the most optimum filler and composition to be used as coating material for carbon steel metal pipelines.

**Keywords** — graphite, graphene oxide, reduced graphene oxide, low-density polyethylene, LDPE

## I. INTRODUCTION

Extensive effort has been done to prevent and mitigate pipeline corrosion, which in turn has led to the entire oil and gas industry to develop various solutions as forms of corrosion prevention and control. Several approaches such as coatings, liners, jackets, and others have been developed to protect the internal surface of pipelines. Nevertheless, many of these techniques are still not fully effective in preventing pipeline corrosion, only reducing the corrosion rate. The most

promising solution so far is the use of the InField Liner (IFL) and similar liners. Despite that, the IFL and other liners alike are considered relatively costly when compared to other methods such as using coatings. This is because the materials used such as polyvinylidene fluoride (PVDF), seamless woven aramid fibres (Kevlar), and thermoplastic polyurethane (TPU) are expensive for pipelines. Thus, there is necessity to develop alternative materials that are more economical while maintaining similar barrier properties to reduce corrosion.

This study aims to solve the problem by producing composites through the incorporation of graphene oxide (GO) and reduced graphene oxide (RGO) into low-density polyethylene (LDPE). LDPE is a good potential material for liners, as it possesses the advantages of low cost, ease of processing, excellent chemical resistance to acids, bases, and solvents. However, some of its disadvantages, such as relatively poor wear resistance and susceptibility to stress-cracking, have limited its wider applications. Thus, polymeric polyethylene-based matrices reinforced with different types of filler have been developed and investigated. GO is one of the promising fillers that can be incorporated into the LDPE matrix to enhance its mechanical properties. However, the hydrophilic nature of GO does not make it a good corrosion repellent. Adsorption of water molecules and corrosive ions are likely to occur in the resulting GO/LDPE composite, which can increase the rate of corrosion. This study suggests in achieving higher mechanical properties while retaining good barrier properties of composites by reducing GO into RGO to promote its hydrophobicity and improve dispersion in the LDPE polymer matrix.

In this research, low-density polyethylene (LDPE) reinforced with graphene oxide (GO) and reduced graphene oxide (RGO) as potential coating materials for carbon steel pipelines were studied. The oxidation and reduction of graphene oxide and reduced graphene oxide from graphite has been conducted and both fillers (GO and RGO) have been characterized to determine their chemical functionality. The LDPE composites containing different loadings of GO and RGO were developed through melt mixing. The processability, mechanical strength, and corrosion resistance were studied and reported.

## II. METHODOLOGY

### A. Synthesis of Graphene Oxide

The GO was prepared through the modified Hummer's method by Yu et al. (2016) with some minor modifications.



10 g of graphite flakes, 6 g of potassium permanganate (KMnO<sub>4</sub>), 4 g of potassium ferrate (K<sub>2</sub>FeO<sub>4</sub>) and 0.01 g of boric acid were dispersed in 200 mL concentrated sulphuric acid (H<sub>2</sub>SO<sub>4</sub>) for 1.5 hours at less than 5 °C. After that, another 5 g of KMnO<sub>4</sub> was added to the mixture before being put into a water bath at 35 °C and stirred for 3 hours to complete the deep oxidation process. 250 mL of deionized water was then slowly added and the temperature adjusted to 95 °C and held for 15 minutes. The diluted suspension will have turned into a brownish colour, which indicates hydrolysis and absolute exfoliation of the intercalated graphite oxide. The brown sulphate solution was treated with 12 mL of 30% hydrogen peroxide (H<sub>2</sub>O<sub>2</sub>) to reduce the oxidant residue and intermediates into soluble sulphate. Following that, the solution was centrifuged at 10,000 rpm for 20 minutes to remove residual graphite supernatant. The solution was washed with 1 mol/L of hydrochloric acid (HCl) and deionized water repeatedly. The product was then suspended in deionized water and freeze-dried. The yield of GO produced is calculated using equations below:

$$\text{Yield} = \left[ \frac{m_f}{m_i} \right] \times 100\%$$

where

$m_f$  = Mass of final product, g

$m_i$  = Mass of feed, g

### B. Synthesis of Reduced Graphene Oxide

The deoxygenation of GO to RGO was carried out by following the method by Habte & Ayele (2019) using L-ascorbic acid as the reducing agent. 400 mg of GO powder was dispersed in 400 mL of deionized water. The amount of GO powder and reductant can be adjusted by following the solution concentration of 0.1 mg/mL. 4 g of L-ascorbic acid was added to this solution and stirred with a magnetic stirrer for 30 minutes at 60 °C. After the reduction process, the resultant mixture solution was washed by centrifugation at 8000 rpm and supernatant removal. That was followed by the addition of excess 30 wt.% H<sub>2</sub>O<sub>2</sub> to the black slurry and stirred for 30 minutes at 60 °C to oxidize any leftover ascorbic acid before being collected after centrifugation at 8000 rpm and washed repeatedly by adding ethanol and deionized water alternately after every supernatant removal for 3 times, respectively. The product was finally dried in an oven overnight at 60 °C to make sure complete drying. The yield of RGO produced is calculated using equations as follows:

$$\text{Yield} = \left[ \frac{m_f}{m_i} \right] \times 100\%$$

where

$m_f$  = Mass of final product, g

$m_i$  = Mass of feed, g

### C. Preparation of Composites

The GO-filled and RGO-filled LDPE composites were prepared by blending LDPE granules with GO and RGO powder respectively. Both composites were blended with the respective GO and RGO filler loadings of 0.5 and 1 wt% each

as seen in **Table-1**, with an additional blend consisting of 100% LDPE prepared as a control specimen. LDPE granules were mechanically mixed with GO powder at a processing temperature of 160 °C and rotating speed of 60 rpm for 8 minutes using a Brabender internal mixer and the steps repeated for LDPE with RGO powder. Two runs of blend-mixing were performed for each composition. Films of the LDPE and composites were obtained by hot pressing the materials by using a hydraulic hot and cold press machine (GT-7014-A30C, GOTECH Testing Machines Inc., Taichung, Taiwan) at 170 °C. The lumps of blends were preheated for 8 minutes, followed by 3 minutes of compression, and 2 minutes of cooling.

Table-1 Filler and Matrix Loadings for Composite Fabrication.

Material	Filler Amount (wt%)	Matrix Amount (wt%)
LDPE	0	100
GO/LDPE	0.5	99.5
GO/LDPE	1	99
RGO/LDPE	0.5	99.5
RGO/LDPE	1	99

### D. Fourier Transform Infrared Spectroscopy (FTIR)

Fourier Transform-Infrared Spectroscopy (FTIR) was conducted by using the Perkin Elmer Spectrum One to determine the chemical functional groups of pristine graphite, GO, and RGO after the synthesis processes.

### E. Thermogravimetric Analysis (TGA)

Thermogravimetric analysis (TGA) is an analytical technique used to determine thermal stability of material and its fraction of volatile components by monitoring the weight change that occurs as a sample is heated at a constant rate. In this study, Mettler Toledo TGA SDTA851E was used to perform the thermogravimetric analysis on the LDPE and composite samples. The operating conditions used were from 25 °C to 900 °C in nitrogen atmosphere with a heating rate of 10 °C/min.

### F. Tensile Test

Five samples were cut into dumbbell shapes following ASTM D638 using a cutter (Leader Technology Scientific (M) Sdn Bhd) for each composition. The thickness of samples at 3 different points were measured by a micrometer and the average value of the thickness was recorded. The samples with gauge length of 26 mm and 3 mm width were subjected to 1200 mm extension range with a 450 N load cell at a crosshead speed of 50 mm/min by using light-weight tensile tester (Tinius Olsen, Model: H10KS-0748, Salfords, UK).

### G. Scanning Electron Microscopy (SEM)

The morphologies for graphite, GO, RGO, LDPE, and composite samples were observed by using JOEL JSM 6701F scanning electron microscope (SEM) with an accelerating voltage of 5 kV. The samples were placed on a disc and held in place using double-sided carbon tape and the fractured

surface was sputtered with a layer of gold prior to observation.

### H. Swelling Test

The swelling behaviour of the samples were measured by the change in mass of samples under the exposure of distilled water and toluene over a period of time under ASTM D570. Ten dumbbell-shaped samples for each composition were cut following ASTM D638 and labelled. The initial weight of the samples were recorded before immersion. After that, five of each of the sample compositions were immersed in distilled water under ambient temperature for 7 days. Next, the samples were removed from the liquids and quickly wiped slightly and weighted. The chemical resistance test was carried out using toluene as immersion solvent under the same conditions as the water absorption test using the remaining five samples of each. The absorption rate is calculated using equations below:

$$\text{Absorption Percentage} = \left[ \frac{m_f - m_i}{m_i} \right] \times 100\%$$

where

$m_i$  = Initial mass of samples, g

$m_f$  = Final mass of samples, g

### I. Corrosion Test

A corrosion test was conducted by coating carbon steel plates with the prepared composites and immersing them in water to observe the corrosion area produced. A quantity of 12 samples were prepared by cutting a large metal plate of 0.2 mm thickness into smaller plates of 4 cm length by 4 cm width. The plates were cleaned and wiped by isopropyl alcohol (IPA). Each of the plates were scaled by drawing grids on one side of the surfaces with a gridline spacing containing boxes of 0.5 cm in length by 0.5 cm in width. 10 of the plates were then coated completely with the LDPE and composites (2 plates for each composite) through a hot and cold press in a 0.5 mm thick mould to ensure a good seal, while 2 plates were left uncoated to be used as control samples. The samples were then immersed in distilled water at 25 °C for 7 days in a dark place. After 7 days, the samples were removed from the solution and wiped by tissue paper. The composite coatings were removed and the appearance of the samples were evaluated after 7 days. The rates of corrosion were then measured from the corroded areas using the formula below:

$$\text{Corrosion Rate} = \left[ \frac{(N_1 + N_2) \times A_1}{P \times A_T} \right] \times 100\%$$

where

$N_1$  = Number of corroded boxes on Plate 1

$N_2$  = Number of corroded boxes on Plate 2

$A_1$  = Area for 1 box, 0.25 cm<sup>2</sup>

$A_T$  = Total surface area of one plate, 64 cm<sup>2</sup>

$P$  = Number of plates, 2

### J. Overall Workflow

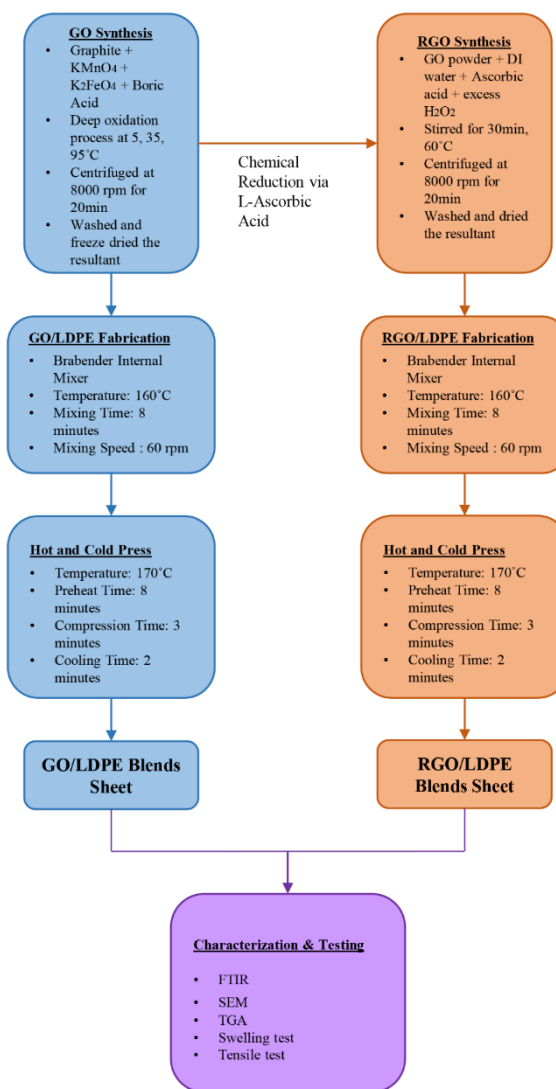


Fig. 1. Overall Methodology Flowchart

## III. RESULTS AND DISCUSSION

### A. Fourier Transform Infrared Spectroscopy (FTIR)

Fig. 2 shows the FTIR spectra of the graphite flakes along with the synthesized GO and RGO powder. Based on the graph, all three materials exhibit broad peaks at the location around 3448 cm<sup>-1</sup>, which has been identified as the O-H stretching functional group (Andrijanto, et al., 2016; Loryuenyong, et al., 2013). An absorption peak at around 1117 cm<sup>-1</sup> of the GO spectra is attributed to the stretching of the C-OH group (Gong, et al., 2015; Tayebi, et al., 2015; Ossson & Bélanger, 2017). The peaks mentioned previously at 3448 cm<sup>-1</sup> and 1117 cm<sup>-1</sup> for all three spectra can also be attributed to the functional groups being more likely to attract water molecules to be adsorbed into the materials (Khalil, 2016; Andrijanto, et al., 2016).

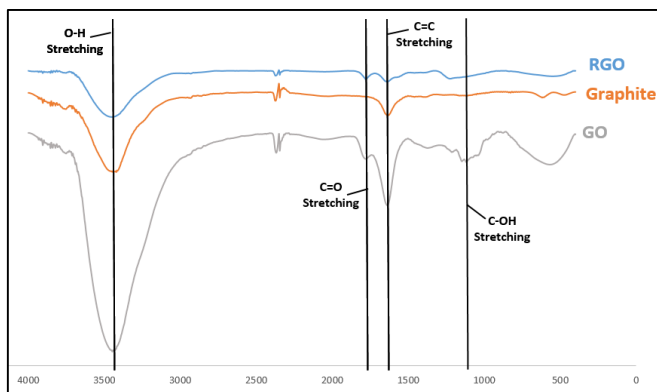


Fig. 2. FTIR of Graphite, GO and RGO.

At around  $1780\text{ cm}^{-1}$ , the GO and RGO spectra exhibit peaks that indicate the presence of C=O stretching of the carboxylic group, with the RGO peak being less intense than the GO peak (Kellici, et al., 2014; Tayebi, et al., 2015). All three spectra show peaks of varying intensities at around  $1638\text{ cm}^{-1}$ , which is assigned to the C=C stretching vibration (Gong, et al., 2015). This indicates that the  $sp^2$  honeycomb-like graphene structure is unchanged throughout the materials even after GO synthesis and reduction processes (Strankowski, et al., 2016). The intense peaks gained after the synthesis of GO at  $3448\text{ cm}^{-1}$ ,  $1780\text{ cm}^{-1}$ , and  $1117\text{ cm}^{-1}$  have greatly disappeared or become less intense once the reduction process has occurred, signalling that many oxygen-containing functional groups have been removed while some residual functional groups only exhibit weaker intensities (Andrijanto, et al., 2016; Tayebi, et al., 2015; Gong, et al., 2015).

### B. Thermogravimetric Analysis (TGA)

TGA has been performed on the aforementioned polymer blends in order to study their thermal stability. The results are summarized in Fig. 3 and Table-2. According to the result graph in Fig. 3, the 100 wt% LDPE and all the composites showed a single step of decomposition. The TG curves show a similar trend in all the samples including LDPE because of the similar degradation mechanisms and chemical bonds in the molecular structures.

The initial temperature of the mass loss or onset temperature ( $T_{\text{onset}}$ ) was observed, and according to Table 4.1, the starting point of the 100 wt% LDPE degradation process began earlier than the polymer blends, decomposing at  $365.72\text{ }^\circ\text{C}$  and consequently completed decomposition at a slightly lower temperature than the polymer blends at  $500.17\text{ }^\circ\text{C}$ . With the incorporation of GO and RGO fillers into the LDPE, the composites indicate a rise in degradation temperatures. This can be seen as all four composites started degrading at an average temperature of about  $380\text{ }^\circ\text{C}$ , with the 0.5 wt% RGO-filled LDPE composite starting to degrade at the highest temperature among the composites at  $387.86\text{ }^\circ\text{C}$ . It also completed its degradation at the highest temperature ( $T_{\text{end}}$ ) among the composites at  $505.90\text{ }^\circ\text{C}$ . The elevated degradation temperature can be attributed by the effect of GO and RGO fillers promoting thermal hindrance (Sabet & Soleimani, 2019). This is caused by the formation of a

protective thermal layer by the fillers to delay oxygen permeation and limit heat diffusion into the LDPE matrix, effectively improving the thermal breakdown endurance and restricting the early degradation of LDPE composites (Yang, et al., 2014; Sabet & Soleimani, 2019; Yee, et al., 2017).

Table-2 Thermogravimetric Analysis of LDPE, GO/LDPE, and RGO/LDPE Composites.

Material	$T_{\text{onset}}$ ( $^\circ\text{C}$ )	$T_{50}$ ( $^\circ\text{C}$ )	$T_{\text{end}}$ ( $^\circ\text{C}$ )	$T_{\text{peak}}$ ( $^\circ\text{C}$ )	Mass loss (%)	Residue (%)
LDPE	365.72	470.08	500.28	476.50	97.22	2.78
GO 0.5 wt%	379.68	475.23	502.73	481.00	96.96	3.03
GO 1.0 wt%	383.80	478.44	502.24	479.83	96.51	3.49
RGO 0.5 wt%	387.86	473.98	505.90	484.67	96.39	3.61
RGO 1.0 wt%	383.82	477.46	501.86	479.33	97.14	2.86

By comparing the char residue after completion of decomposition, the 100 wt% LDPE has the least residue at 2.78 %. The 0.5 wt% GO, 1 wt% GO, 0.5 wt% RGO, and 1 wt% RGO have char residue yields of 3.03 %, 3.49 %, 3.61 %, 2.86 %, respectively. The higher amount of char yields by the composites were probably due to the presence of GO and RGO in the LDPE, which caused carbonization on the surface of the polymer or additionally, the high heat resistance of the fillers allowed for them to be partially unburned (Yusof, et al., 2018). Thus, it can be deduced that the addition of GO and RGO as fillers are able to improve the thermal stability of LDPE, but the difference between the loadings (0.5 wt% and 1 wt%) for both fillers does not significantly affect the thermal stability.

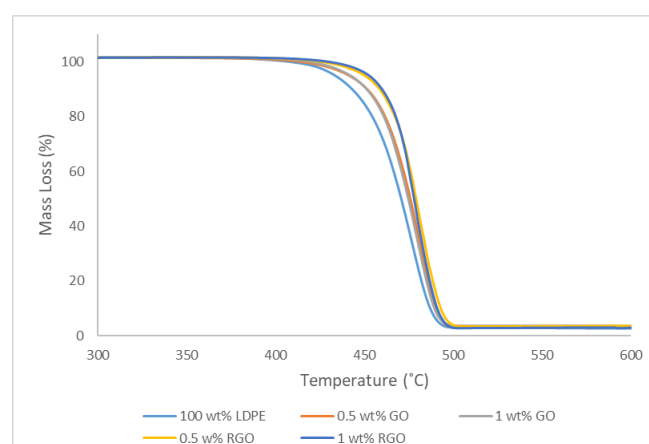


Fig. 3. TGA curve of LDPE, GO/LDPE, and RGO/LDPE Composites

### C. Tensile Tests

Young modulus is a measurement in which the elastic stress and strain of a material is used to describe its relative stiffness and is calculated by the stress to strain value ratio (Vaidya & Pathak, 2019). Fig. 4 shows the effect of different filler loadings on the Young modulus of LDPE composites. According to graph, the Young modulus is increased with the

addition of fillers. The 1 wt% RGO-filled LDPE composite has the highest stiffness among the composites (183.9 MPa) while the 0.5 wt% RGO-filled LDPE composite has the lowest stiffness among the composites (162 MPa). This indicates that the addition of 0.5 wt% does not improve the stiffness by much, but with 1 wt% of RGO, it significantly increased the Young modulus value by 25 % compared to pure LDPE (147.08 MPa).

On the other hand, the 0.5 wt% and 1 wt% GO-filled LDPE composites have Young modulus values of 171.6 MPa and 175.6 MPa respectively, which are higher than the 100 wt% LDPE and 0.5 wt% RGO/LDPE, but lower than the 1 wt% RGO/LDPE composite. The 0.5 wt% GO/LDPE improves the Young modulus of LDPE by 17 %. However, when the GO loading was increased to 1 wt%, there is only a 19 % improvement in the Young modulus observed. This is only a 2 % difference than the 0.5 wt% loading of GO. This finding suggests that the RGO has a more significant effect on the Young modulus of LDPE when increasing the loading. This can be evidenced from the difference of 15 % Young modulus between the 0.5 wt% RGO/LDPE and the 1 wt% RGO/LDPE composites. Furthermore, the increment of Young modulus values with both fillers indicates that there could be an excellent interfacial adhesion between the fillers and LDPE matrix, which helps to overcome dispersion problems and improve the mechanical properties of the composites in comparison with the 100 wt% LDPE (Wypych, 2016).

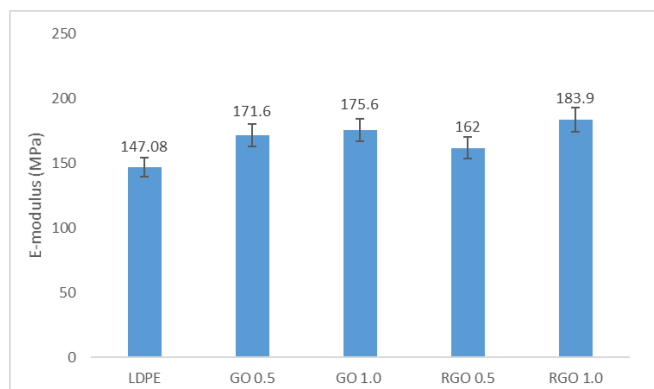


Fig. 4. Young Modulus Results for LDPE, GO/LDPE, and RGO/LDPE Composites

Elongation-at-break (Eb) or fracture strain is a measurement to assess the breaking point of a material while being stretched by measuring the ratio between the material's initial length and changed length after breakage and is expressed in the terms of percentage of its original length (Petroudy, 2017). High elongation values before breaking are attributed to high ductility in the tested materials (Shebani, et al., 2018). **Fig. 5** shows the elongation-at-break of LDPE and its composites with different GO and RGO loadings. As seen in **Fig. 5**, the elongation-at-break values of the composites decreased gradually as the GO and RGO filler loading increased. This is in line with the results of increasing Young modulus values, which indicate the increase in stiffness of the composites (Tayebi, et al., 2015). This is due to the restriction

of polymer chain movement with the presence of filler particles. The particles tend to penetrate in between the polymer chains and reduce the flexibility for chain rearrangement. This subsequently reduces deformability and improves the stiffness of the composites (Wypych, 2016).

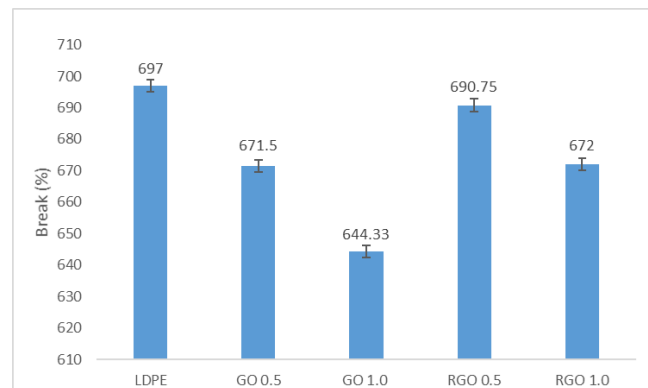


Fig. 5. Elongation at Break Results for LDPE, GO/LDPE, and RGO/LDPE Composites

On the other hand, the most important tensile property that needs to be measured is the ultimate tensile strength (UTS), which is the maximum stress or load that a material can withstand before breaking (Singh, 2012). **Fig. 6** shows the UTS values of LDPE and its composites with different GO and RGO filler loadings. From **Fig. 6**, it can be observed that the 1 wt% GO-filled LDPE composite exhibited the lowest UTS as compared to the LDPE and other composites. This is possibly due to the particles of GO not being sufficiently dispersed and wetted into the polymer matrix. Poor wetting of GO by LDPE results in agglomeration and inefficient stress transfer at the point of breakage (Wang, et al., 2011). Thus, further addition of GO above 0.5 wt% results in even an even more aggravated effect of agglomeration and reduction in UTS.

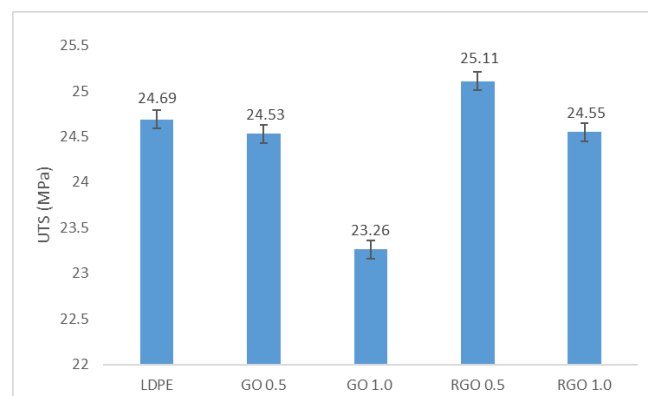


Fig. 6. Ultimate Tensile Strength Results for LDPE, GO/LDPE, and RGO/LDPE Composites

Contrarily, the 0.5 wt% RGO-filled LDPE composite on the other hand has the highest UTS compared to LDPE and the other composites. This can be attributed to the strong interfacial bonding between the RGO filler and polymer matrix as compared to GO and LDPE matrix (He &

Tjong, 2016). Besides, the reduction of hydroxyl groups in RGO as evidenced from the FTIR analysis proves that RGO has a better interfacial adhesion with LDPE as compared to GO. The enhancement of interfacial adhesion results in a more efficient stress transfer between RGO and LDPE. However, further increasing the RGO loading to 1 wt% results in a similar reducing trend as that of GO in LDPE. At higher RGO loading of 1 wt%, the composite tends to become highly stiff and thus, the particles could not rearrange upon stress application. This results in the deterioration of the UTS due to the low resistance towards crack propagation of the composite system. This can be evidenced from the tensile fracture surface of the RGO/LDPE composite containing 1 wt% RGO which is smooth, indicating a brittle fracture with low resistance towards crack propagation.

#### D. Scanning Electron Microscopy (SEM)

The morphological analysis of graphite flakes, GO, and RGO was carried out to observe the difference on the characteristics of these fillers in terms of particle shape, particle distribution, and surface morphology, which could influence the properties of the LDPE composites. Besides, morphological analysis was also carried out on the tensile fracture surface of LDPE and GO/RGO-filled LDPE composites to observe the effect of GO and RGO addition on the surface morphology, such as surface roughness, matrix tearing, filler dispersion, and interfacial adhesion between the fillers and LDPE matrix. **Fig. 7 (a)** and **(b)** show the SEM images of graphite, whereas **Fig. 8 (a)** and **(b)** show the SEM images of GO, and **Fig. 8 (c)** and **(d)** show the SEM images of RGO. According to **Fig. 7**, it can be seen that the graphite consists of flake-like grains with smooth and jagged edges. Grain and gas evolution mismatch during the processing of graphite by the manufacture might have caused the material to have a porous structure (Kamali & Fray, 2015).

Whereas, from **Fig. 8 (a)** and **(b)**, it shows that the synthesized GO particles are in closely packed layers with rippling and crumpling in the structures. Such structure is possibly due to deformation caused by the exfoliation and restacking during the synthesis process (Fu, et al., 2013). Another possibility to the rough surface of the GO would be by the freeze-drying treatment being carried out after the synthesis processes (Hayes, et al., 2014). The morphology of GO shows certain similarities to the graphite morphology due to its smooth grain structure. However, the GO particles tend to be more shaped in flat sheets, which are stacked close to one another to form more porous structures as compared to graphite.

On the other hand, RGO exhibits smooth surfaced structures with random agglomeration that have folds and distinct edges, typically seen in graphene-like morphology as can be observed from **Fig. 8 (c)** and **(d)**. The morphology of RGO resembles the morphology of GO. However, the stacking of the RGO flat sheets are much looser and there are larger gaps in between the stacks. This suggests that RGO could allow more exfoliation with the LDPE chain and create larger surface areas for polymer adhesion (Junaidi, et al., 2018). This result is in line with the higher UTS of the

RGO/LDPE composites as compared to the GO/LDPE composites and 100 wt% LDPE.

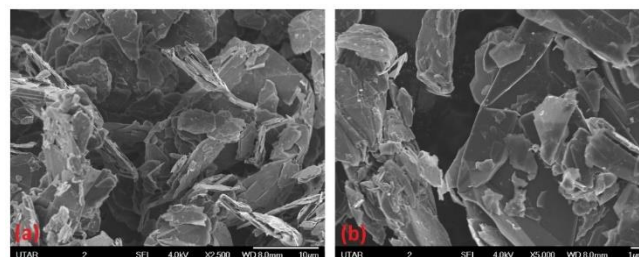


Fig. 7. SEM Images of Graphite at Magnifications of (a) 2500 and (b) 5000

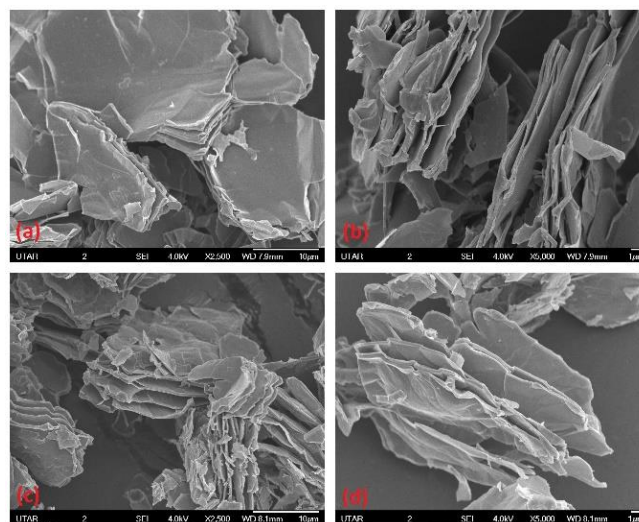


Fig. 8. SEM Images of GO at Magnifications of (a) 2500 and (b) 5000; RGO at Magnifications of (c) 2500 and (d) 5000

**Fig. 9** shows the SEM images of the tensile fracture surface of the LDPE composites at different GO and RGO loadings. **Fig. 9 (a)** shows the SEM image of the tensile fracture surface of 100 wt% LDPE. The fracture surface exhibits a relatively smooth surface with possible microcracks. There is no visible matrix tearing observed, which indicates that LDPE has low resistance towards crack propagation. The application of stress results in homogeneous stress transfer throughout the matrix, producing a smooth fracture surface with smaller microcracks due to stress resistance.

Meanwhile, from **Fig. 9 (b)** and **(c)**, the structures of GO/LDPE composites with 0.5 wt% and 1 wt% GO loadings can be seen, respectively. Several agglomeration spots can be seen in both of the GO/LDPE composites. The presence of hydroxyl groups in GO makes the particles incompatible to LDPE. Thus, the agglomerations occurred due to the poor adhesion and dispersion of the filler within some parts of the polymer matrix, as well as the large amount of filler weight percentage used (Le & Huang, 2015). Besides that, visible surface cracks and matrix tearing can be seen on both of the GO/LDPE composites, which suggest high resistance towards crack propagation of the LDPE in the presence of GO

particles. The mobility of the chains has been restricted due to the presence of GO particles. Therefore, the chains possess high resistance towards crack propagation before the matrix fails to hold the stress and breaks into string-like structures. This is in line with the increasing Young modulus, which increased for both of the GO/LDPE composites.

**Fig. 9 (d) and (e)** show the tensile fracture surfaces of RGO/LDPE composites at 0.5 wt% and 1 wt%, respectively. It can be observed from the figures that there is no visible agglomeration of the RGO on the surface of both of the RGO/LDPE composites. The RGO particles are fully embedded on the LDPE matrix with no phase separation between RGO and LDPE. This indicates that there is a good dispersion of RGO in LDPE and better adhesion between the RGO and LDPE matrix, promoting the mechanical properties of composites.

However, when comparing between the tensile fracture surfaces of the 0.5 wt% RGO/LDPE and 1 wt% RGO/LDPE composites as in **Fig. 9 (d) and (e)**, respectively, it can be seen that the surface of 0.5 wt% RGO/LDPE is much rougher than the 1 wt% RGO/LDPE. This observation reveals that LDPE with 0.5 wt% RGO has a higher resistance towards crack propagation than the composite containing 1 wt% RGO. The smooth fracture surface of the 1 wt% RGO/LDPE could be due to the high stiffness of the composites at higher RGO loading, which hinders the deformation of LDPE chains and promotes brittle fracture. This observation is in line with the higher Young modulus and lower UTS and Eb of the 1 wt% RGO/LDPE composite as compared to the 0.5 wt% RGO/LDPE composite.

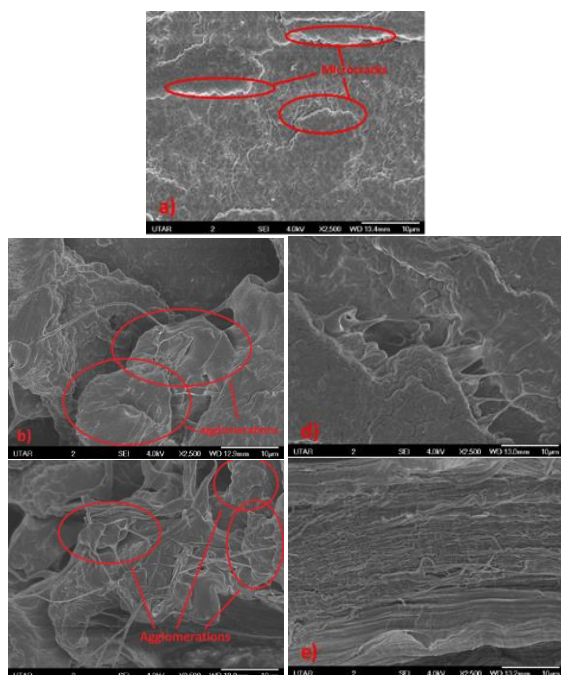


**Fig. 9.** Tensile Fracture Surface Images at Magnification of 2500 for (a)100 wt% LDPE, (b) 0.5 wt% GO/LDPE, (c) 1

wt% GO/LDPE, (d) 0.5 wt% RGO/LDPE, and (e) 1 wt% RGO/LDPE

### E. Swelling Tests

Swelling tests have been conducted using distilled water and toluene to determine the effect of GO and RGO addition on the resistance of the LDPE composites against water and chemical absorption. A higher absorption rate indicates low resistance towards water or chemical absorption and consequently signifies that the composites have poor water and chemical stability. **Fig. 10** depicts the water absorption rate of LDPE and its composites with different GO and RGO filler loadings. It can be seen from **Fig. 10** that the addition of both types of fillers has reduced the water absorption rate of LDPE composites as compared to the 100 wt% LDPE. The addition of 0.5 wt% and 1 wt% of GO had lowered the water absorption rate from 0.87 % for the 100 wt% LDPE to 0.48 % and 0.45 %, respectively. On the other hand, it can be seen that the 0.5 wt% RGO/LDPE composite has the lowest water absorption rate of 0.25 %, while the addition of 1 wt% RGO to LDPE decreased the water absorption rate from 0.87 % to 0.28 %.

Meanwhile, when comparing the GO/LDPE and RGO/LDPE composites, it can be observed that both 0.5 wt% GO/LDPE and 1 wt% GO/LDPE possess higher water absorption rates as compared to RGO/LDPE composites of similar loadings. These results can be related to the high hydrophilic nature of GO as compared to RGO. The FTIR analysis has proven that the hydroxyl groups of GO has been reduced in RGO during the reduction process. Thus, RGO has a lower tendency to interact with water molecules as compared to GO. Besides, better dispersion and interfacial adhesion between RGO and LDPE also prevent penetration of water molecules into the LDPE matrix as compared to the GO-LDPE matrix surface.

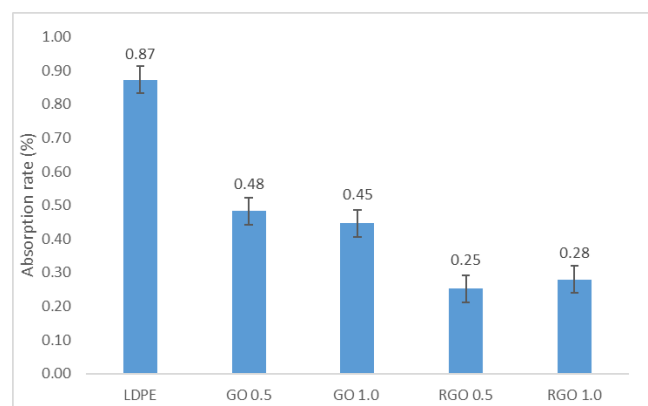


**Fig. 10.** Water Absorption Results of LDPE and Composites

On the other hand, the toluene absorption rate of LDPE and its composites containing different loadings of GO and RGO fillers are illustrated in **Fig. 11**. It can be seen from **Fig. 11** that the 100 wt% LDPE absorbs a high amount of toluene with an absorption rate of 18.59%. This is because LDPE has a limited resistance against aromatic solvents and is especially vulnerable to toluene (Wong, et al., 2014). With

the addition of 0.5 wt% GO, LDPE tends to absorb slightly more toluene as can be seen from **Fig. 11**. The absorption rate of 0.5 wt% GO/LDPE is 18.62% as compared to 18.59% for the 100 wt% LDPE. The poor adhesion between GO and LDPE results in easier penetration for the toluene molecules into the LDPE matrix. However, increasing the GO loading to 1 wt% results in a significant reduction in toluene absorption rate from 18.62% to 17.97%. The hydrophilic nature of GO as compared to LDPE results in poor interaction with non-polar solvents such as toluene (Klechikov, et al., 2015). This causes repulsion between the toluene molecules and GO particles in the LDPE matrix. Thus, at a higher GO loading of 1 wt%, the toluene molecules were not able to penetrate into and intercalate with the GO/LDPE molecules easily, consequently resulting in a reduction in toluene absorption rate.

Meanwhile, the addition of RGO showed a significant reduction in toluene absorption rate for both of the 0.5 wt% and 1 wt% loadings. The 0.5 wt % RGO/LDPE composite exhibited an absorption rate of 18 % as compared to 18.59 % for 100 wt% LDPE. Whereas, increasing the RGO loading to 1 wt% showed a further reduction in toluene absorption rate to 17.78 %. Improved dispersion of RGO in LDPE and better interfacial adhesion between hydrophobic RGO and LDPE could be responsible for the reduction in toluene absorption rate. RGO particles have better interfacial adhesion as proven from the increasing UTS and SEM morphological observation. Thus, the penetration of toluene molecules into LDPE would have been hindered in the presence of RGO.

Furthermore, when comparing the effect of GO and RGO addition, it can be seen that RGO showed a better resistance towards toluene absorption as compared to GO. This is because RGO/LDPE composites showed lower toluene absorption rate as compared to GO/LDPE composites at similar filler loadings. A study conducted by Awaja, et al., (2016) suggests that there is a possibility of microcrack formation in the structure of LDPE during processing. The hydrophobic nature of LDPE would lead to formation of microcracks, especially during the melt mixing and compression moulding process. The presence of contaminants and impurities could initiate the formation of microcracks, which promotes the penetration of both water and toluene molecules (Mallik, et al., 2015). Similarly, there were also other studies that reported on the formation of microvoids in polymers during the melting and reshaping process caused by the evaporation of volatile impurities. The presence of microvoids thus further allows the absorption of water and other solvents into the polymer matrix (Halip, et al., 2019; Chu, et al., 1994).

Additionally, the presence of GO, while hydrophilic in nature, can fill up the microcracks and microvoids in the LDPE, which improves surface smoothness and reduces the water absorption rate of the composite (Mallik, et al., 2015). Consequently, the use of RGO then allows for even lower water absorption rate due to its hydrophobic nature. This can also be observed through the toluene absorption test, as the presence of GO at higher loading (1 wt%) and RGO (at both

loadings) can significantly reduce the toluene's permeability into the polymer (Wang, et al., 2011). In conclusion, RGO/LDPE composite has a greater moisture and solvent resistance compared to the 100 wt% LDPE and GO/LDPE composite.

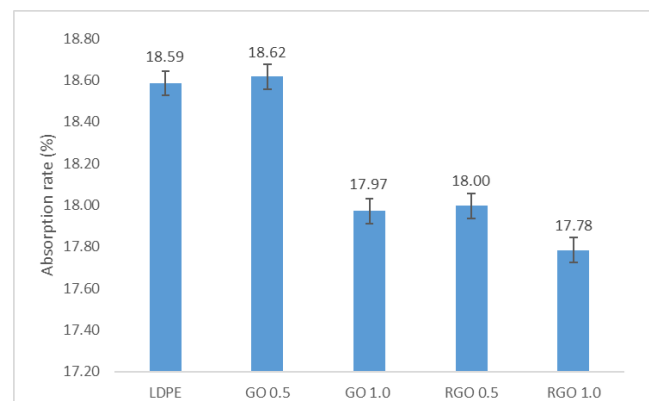


**Fig. 11.** Toluene Absorption Results of LDPE and Composites.

#### **F. Corrosion Test**

A corrosion test was conducted to determine the corrosion resistance of a material under certain environment conditions. It helps to evaluate the performance of materials under simulated or real conditions (Bardal, 2003). **Fig. 12** shows the average corrosion rates of coated and uncoated metal plates submerged in water for 7 days while **Table 3** shows the tabulated data of the corroded areas of the metal plates.

**Fig. 13** shows the physical appearance of the uncoated metal plates after being submerged in water for 7 days. It can be observed that the uncoated metal plates became fully corroded with a corrosion rate of 100% after being exposed to water for 7 days. Meanwhile, **Fig. 14** shows the corrosion on metal plates coated with the 100 wt% LDPE. For these 100 wt% LDPE-coated metal plates, the corroded region was reduced significantly with a corrosion rate of about 12.5 %. The reduction in corrosion rate could be due to the good barrier properties of LDPE, which has good strength as observed from the tensile test results and adequate moisture resistance when the surface is smooth with little amount of microcracks.

**Fig. 15** shows the metal plates coated with the 0.5 wt% GO/LDPE composite when submerged in water, whereas **Fig. 16** shows the corrosion on metal plates coated with the 1 wt% GO/LDPE composite. From **Table 3**, it can be observed that the corrosion rate on the metal plates reduced slightly to 11.72 % when the 0.5 wt% GO/LDPE composite was used as the coating. This indicates that the GO has a slight effect in improving the barrier properties of the LDPE. However, the metal plates coated with 1 wt% GO/LDPE seem to have worse performance as the corrosion rate increased to 16.41 %. This may be due to the composite rupturing during the coating process, resulting in water penetrating more easily and reducing its performance. This can be evidenced from the tensile results when looking at the 1 wt% GO/LDPE having the lowest ultimate tensile strength

and elongation at break while having high stiffness, which could easily rupture during the coating process.

**Fig. 17** shows the corrosion on metal plates coated with the 0.5 wt% RGO/LDPE composite when submerged in water, while **Fig. 18** shows the corrosion on metal plates coated with the 1 wt% RGO/LDPE composite. As can be seen from **Table-3**, the plates coated with 0.5 wt% RGO/LDPE composite exhibited a significantly lower corrosion rate of 7.81% than the previous liners, as one of plates does not show any evidence of corrosion. This is a good indication that the presence of RGO as the filler in LDPE can improve the performance by 4.69 % as compared to the 100 wt% LDPE coating. On the other hand, it can be observed that the metal plates coated with the 1 wt% RGO/LDPE composite exhibited the greatest corrosion resistance with a corrosion rate of 0 %, as both plates have no corroded regions. The results obtained clearly signify that the presence of GO and RGO fillers in LDPE greatly improve its moisture resistance. While it can also be concluded that the use of RGO as a filler with the appropriate loading can even prevent corrosion altogether, giving metallic materials a high corrosion resistance and longer lifespan.

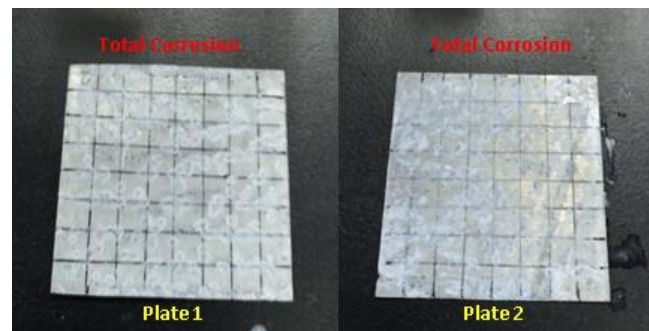


Fig. 13. Uncoated Metal Plates

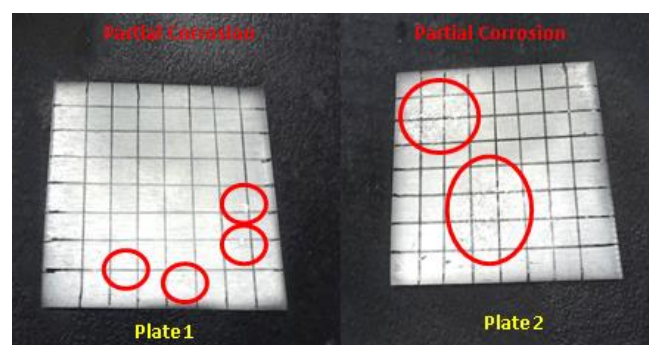


Fig. 14. 100 wt% LDPE-Coated Metal Plates

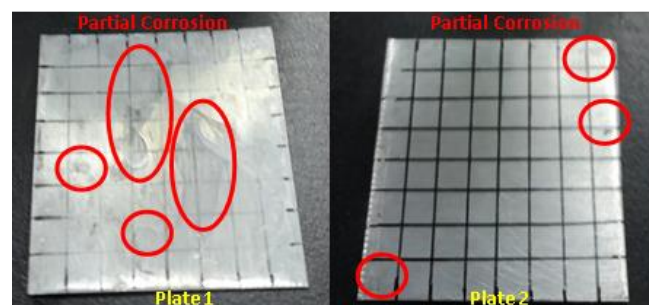


Fig. 15. 0.5 wt% GO/LDPE-Coated Metal Plates

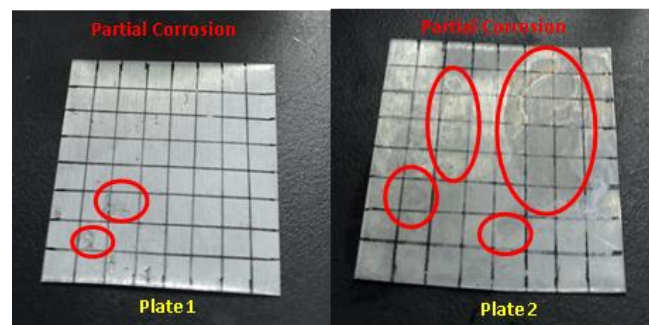


Fig. 16. 1 wt% GO/LDPE-Coated Metal Plates

Table-3 Data for Corroded Areas on Metal Plates.

Coating on Plates	Plate 1 Corroded Boxes	Plate 1 Corrosion Area (cm <sup>2</sup> )	Plate 2 Corroded Boxes	Plate 2 Corrosion Area (cm <sup>2</sup> )	Average Corrosion Area (cm <sup>2</sup> )	Corrosion Rate (%)
No Coating	64	16.00	64	16.00	16.000	100
100 wt% LDPE	4	1.00	12	3.00	2.000	12.50
0.5 wt% GO/LDPE	12	3.00	3	0.75	1.875	11.72
1 wt% GO/LDPE	2	0.50	19	4.75	2.625	16.41
0.5 wt% RGO/LDPE	10	2.50	0	0	1.250	7.81
1 wt% RGO/LDPE	0	0	0	0	0	0

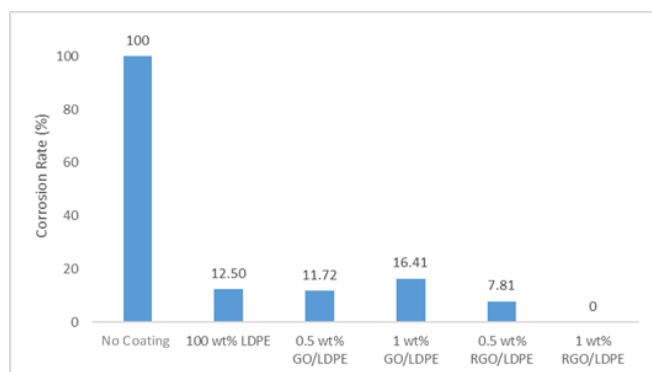


Fig. 12. Corrosion Rates of Metal Plates with Different Coatings

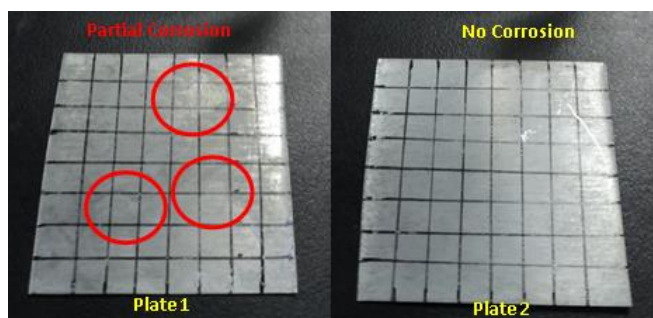


Fig. 17. 0.5 wt% RGO/LDPE-Coated Metal Plates

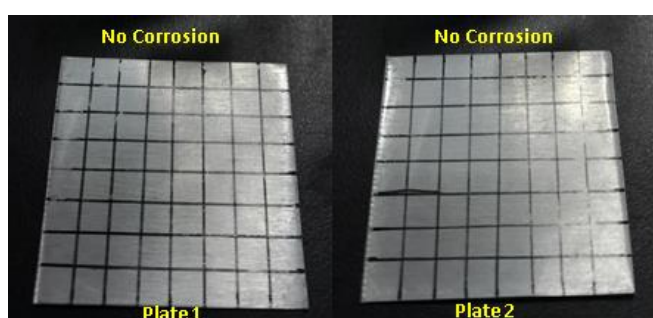


Fig. 18. 1 wt% RGO/LDPE-Coated Metal Plates

#### IV. CONCLUSION

In conclusion, graphene oxide was successfully synthesized from natural graphite flakes by using an improved Hummers method with a 120 % yield and later successfully reduced into reduced graphene oxide by chemical reduction using ascorbic acid with an 83 % yield. Characterization of the graphite, GO, and RGO using FTIR revealed the presence of oxygenated functional groups in the GO and the removal of oxygenated functional groups in the RGO. RGO showed a reduction in hydroxyl groups, which makes it hydrophobic and more compatible for use as filler in LDPE.

LDPE composites containing 0.5 wt% and 1 wt% of GO and RGO have been successfully developed through melt mixing using a Brabender internal mixer at a mixing temperature of 160 °C, mixing speed of 60 rpm, and mixing time of 8 minutes. The compounded LDPE, GO/LDPE, and RGO/LDPE composites were then compressed into thin composite sheets using a hot and cold pressing machine at a temperature of 170 °C with a preheating time, hot pressing time, and cooling time of 8 minutes, 3 minutes, and 2 minutes, respectively. The TGA results showed that there was an increase in thermal stability with the addition of filler and that the 1 wt% RGO/LDPE composite had the greatest thermal stability. It was also found that the mechanical strength of the composites were improved with the addition of the GO and RGO fillers. The RGO/LDPE composites exhibited good mechanical properties as compared to 100 wt% LDPE and the GO/LDPE composites as evidenced from the increased tensile strength and Young modulus as well as comparable elongation at break.

Morphological analysis of tensile fracture surfaces confirmed the presence of agglomeration for both 0.5 wt%

and 1 wt% GO/LDPE composites, which could possibly affect the mechanical strength, water, and toluene absorption as well as corrosion resistance of the GO/LDPE composites. Meanwhile, RGO/LDPE composites showed smoother structural morphology with no agglomeration, indicating good dispersion of RGO particles in LDPE and improved interfacial bonding of the filler and matrix. These factors could be responsible in improving the mechanical strength of the RGO/LDPE composites. Besides, the RGO/LDPE composites had greater improvement in moisture and solvent resistance as compared to 100 wt% LDPE and GO/LDPE composites.

Finally, the corrosion test also proved that the metal plates coated with the 1 wt% RGO/LDPE composite exhibits the greatest corrosion resistance with a corrosion rate of 0%. The addition of GO and RGO as filler has improved the mechanical strength and barrier properties of LDPE with a more significant effect shown by RGO as compared to GO. Thus, the RGO/LDPE composites at 1 wt% RGO loading is the most optimum filler and composition to be used as coating material for carbon steel metal pipelines.

#### V. ACKNOWLEDGEMENT

The author wishes to express gratitude to Dr Mathialagan Muniyadi and all UTAR lab officers for their support and advices. The author also extends gratitude towards Universiti Tunku Abdul Rahman to allow for this research to happen.

#### VI. REFERENCES

- Andrijanto, E., Shoelarta, S., Subiyanto, G., & Rifki, S. (2016). Facile synthesis of graphene from graphite using ascorbic acid as reducing agent. New York: AIP Publishing.
- Awaja, F., Zhang, S., Tripathi, M., Nikiforov, A., & Pugno, N. (2016). Cracks, microcracks and fracture in polymer structures: Formation, detection, autonomic repair. *Progress in Materials Science*, 83, 536-573.
- Bardal, E. (2003). Corrosion Testing, Monitoring and Inspection. In *Corrosion and Protection* (pp. 219-235). London: Springer.
- Chu, F., Yamaoka, T., Ide, H., & Kimura, Y. (1994). Microvoid formation process during the plastic deformation of  $\beta$ -form polypropylene. *Polymer*, 35(16), 3442-3448.
- Fu, C., Zhao, G., Zhang, H., & Li, S. (2013). Evaluation and Characterization of Reduced Graphene Oxide Nanosheets as Anode Materials for Lithium-Ion Batteries. *International Journal of Electrochemical Science*, 8, 6269-6280.
- Gong, Y., Li, D., Fu, Q., & Pan, C. (2015). Influence of graphene microstructures on electrochemical performance for supercapacitors. *Progress in Natural: Science Materials International*, 25(5), 379-385.
- Habte, A. T., & Ayele, D. W. (2019). Synthesis and Characterization of Reduced Graphene Oxide (rGO) Started from Graphene Oxide (GO) Using the Tour Method with Different Parameters. *Advances in Materials Science and Engineering*, 2019, 1-9.



- Halip, J. A., Hua, L. S., Ashaari, Z., Tahir, P. M., Chen, L. W., & Uyup, M. K. (2019). 8 - Effect of treatment on water absorption behavior of natural fiber-reinforced polymer composites. In M. Jawaid, M. Thariq, & N. Saba (Eds.), *Mechanical and Physical Testing of Biocomposites, Fibre-Reinforced Composites and Hybrid Composites* (pp. 141-156). Cambridge: Woodhead Publishing.
- Hayes, W. I., Joseph, P., Mughal, M. Z., & Papakonstantinou, P. (2014). Production of reduced graphene oxide via hydrothermal reduction in an aqueous sulphuric acid suspension and its electrochemical behaviour. *J Solid State Electrochem.*
- He, L., & Tjong, S. C. (2016). 7 - Preparation of Nanocomposites. In J. Parameswaranpillai, N. Hameed, T. Kurian, & Y. Yu (Eds.), *Nanocomposite Materials: Synthesis, Properties and Applications* (pp. 147-172). Florida: CRC Press.
- Junaidi, N. F., Othman, N. H., Ismail, I. N., Alias, N. H., Zaman, M., Shahrudi, . . . Abdullah, W. F. (2018). Reduction of Sonication-Assisted Graphene Oxide via Chemical and Thermal Treatments. *International Journal of Engineering & Technology*, 7, 217-222.
- Kamali, A. R., & Fray, D. J. (2015). Large-scale preparation of graphene by high temperature insertion of hydrogen into graphite. *Nanoscale*(26), 11310-11320.
- Kellici, S., Acord, J., Ball, J., Reehal, H. S., Morgan, D., & Saha, B. (2014). A single rapid route for the synthesis of reduced graphene oxide with antibacterial activities. *RSC Advances*, 4(29), 14858-14861.
- Khalil, D. (2016). Graphene oxide: a promising carbocatalyst for the regioselective thiocyanation of aromatic amines, phenols, anisols and enolizable ketones by hydrogen peroxide/KSCN in water. *New Journal of Chemistry*, 40(3), 2547-2553.
- Klechikov, A., Yu, J., Thomas, D., Sharifia, T., & Talyzin, A. V. (2015). Structure of graphene oxide membranes in solvents and solutions. *Nanoscale*, 7, 15374-15384.
- Le, M.-T., & Huang, S.-C. (2015). Thermal and Mechanical Behavior of Hybrid Polymer Nanocomposite Reinforced with Graphene Nanoplatelets. *Materials*, 8, 5526-5536.
- Loryuenyong, V., Totepvimarn, K., Eimburanapravat, P., Boonchompoo, W., & Buasri, A. (2013). Preparation and Characterization of Reduced Graphene Oxide Sheets via Water-Based Exfoliation and Reduction Methods. *Advances in Materials Science and Engineering*, 2013, 1-5.
- Mallik, A., Barik, A. K., & Pal, B. (2015). Comparative studies on physico-mechanical properties of composite materials of low density polyethylene and raw/calcined kaolin. *Journal of Asian Ceramic Societies*, 3(2), 212-216.
- Ossonon, B. D., & Bélanger, D. (2017). Synthesis and characterization of sulfophenyl-functionalized reduced graphene oxide sheets. *RSC Advances*, 7(44), 27224-27234.
- Petroudy, S. R. (2017). 3 - Physical and mechanical properties of natural fibers. In M. Fan, & F. Fu (Eds.), *Advanced High Strength Natural Fibre Composites in Construction* (pp. 59-83). Cambridge: Woodhead Publishing.
- Sabet, M., & Soleimani, H. (2019). Inclusion of graphene on LDPE properties. *Heliyon*, 5(7), 1-10.
- Singh, R. (2012). Chapter 11 - Mechanical Properties and Testing of Metals. In *Applied Welding Engineering: Processes, Codes, and Standards* (pp. 87-94). Oxford: Butterworth-Heinemann.
- Strankowski, M. B., Bodarczyk, D. W., Piszczyk, A., & Strankowska, J. (2016). Polyurethane Nanocomposites Containing Reduced Graphene Oxide, FTIR, Raman, and XRD Studies. *Journal of Spectroscopy*, 2016, 1-6.
- Tayebi, M., Ahmad Ramazani Saadat Abadi, M. T., & Tayyebi, A. (2015). LDPE/EVA/graphene nanocomposites with enhanced mechanical and gas permeability properties. *Polymers for Advanced Technologies*, 26(9), 1083-1090.
- Vaidya, A., & Pathak, K. (2019). 17 - Mechanical stability of dental materials. In A. M. Asiri, Inamuddin, & A. Mohammad (Eds.), *Applications of Nanocomposite Materials in Dentistry* (pp. 285-305). Cambridge: Woodhead Publishing.
- Wang, J., Xu, C., Hu, H., & Wan, L. (2011). Synthesis, mechanical, and barrier properties of LDPE/graphene nanocomposites using vinyl triethoxysilane as a coupling agent. *Journal of Nanoparticle Research*, 13(2), 869-878.
- Wong, S. L., Ngadi, N., & Abdullah, T. A. (2014, November). Study on Dissolution of Low Density Polyethylene (LDPE). *Applied Mechanics and Materials*, 695, 170-173.
- Wypych, G. (2016). The Effect of Fillers on the Mechanical Properties of Filled Materials. In *Handbook of Fillers (Fourth Edition)* (pp. 467-531).
- Yang, X., Mei, T., Yang, J., Zhang, C., Lv, M., & Wang, X. (2014). Synthesis and characterization of alkylamine-functionalized graphene for polyolefin-based nanocomposites. *Applied Surface Science*, 205, 725-731.
- Yee, T. G., Ong, H. L., Bindumadhavan, K., & Doong, R.-a. (2017). Unveiling the thermal kinetics and scissoring mechanism of neolaty polyethylene/reduced graphite oxide nanocomposites. *Journal of Analytical and Applied Pyrolysis*, 123, 20-29.
- Yu, H., Zhang, B., Bulin, C., Li, R., & Xing, R. (2016). High-efficient Synthesis of Graphene Oxide Based on Improved Hummers Method. *Scientific Reports*, 6(36143), 1-7.
- Yusof, M., Rahman, N. N., Sulaiman, S., Sofian, A., Desa, M. M., & Izirwan, I. (2018). Development of Low Density Polyethylene /Graphene Nanoplatelets with Enhanced. *International Conference on Mechanical and Intelligent Manufacturing Technologies*, 6-9.

